4818 *Organometallics* **2010,** *29,* 4818–4828
DOI: 10.1021/om100148z

ORGANOMETALLICS
Article

From Allenes to Edge-Bridging Allyl Ligands or Face-Capping Alkenyl Ligands on a Triruthenium Hydrido Carbonyl Cluster: An Experimental and DFT Computational Study†

Javier A. Cabeza,*,‡ Ignacio del Río,‡ José M. Fernández-Colinas,‡ Enrique Pérez-Carreño,§ and Digna Vázquez-García‡

‡*Departamento de Química Orgánica e Inorgánica-IUQOEM, Universidad de Oviedo-CSIC, E-33071 Oviedo, Spain, and* §*Departamento de Química Física y Analítica, Universidad de Oviedo, E-33071 Oviedo, Spain*

Received February 24, 2010

Terminal allenes, $H_2CCCR^1R^2$ ($R^1 = R^2 = Me$; $R^1 = SiMe_3$, $R^2 = Me$; $R^1 = CO_2Et$, $R^2 = H$; $R^1 = Cy$, $R^2 = H$), react with the hydrazido-capped hydrido carbonyl triruthenium complex $[Ru_3(\mu\text{-}H)(\mu_3\text{-}\kappa^2\text{-}HNNMe_2)(CO)_9]$ (**1**) in THF at reflux temperature to give the allyl-bridged derivatives $[Ru_3(\mu\text{-}\kappa^3\text{-}H_2CCHCR^1R^2)(\mu_3\text{-}\kappa^2\text{-}HNNMe_2)(\mu\text{-}CO)_2(CO)_6]$, as mixtures of *syn*-allyl and *anti*-allyl isomers when $R^1 \neq R^2$. These reactions also produce a small amount of an alkenyl-capped derivative, $[Ru_3(\mu_3\text{-}\kappa^2\text{-}HNNMe_2)(\mu_3\text{-}\kappa^2\text{-}MeCCHR^1)(\mu\text{-}CO)_2(CO)_6]$, when monosubstituted allenes ($R^2 = H$) are used. Density functional theory calculations have shown that the reactions that give edge-bridging allyl or face-capping alkenyl derivatives from compound **1** and allene are multistep processes. In both cases, the first step, a bimolecular allene for CO substitution, is rate-limiting. The way the allene approaches the cluster complex determines the formation of an allyl or alkenyl product, since this fact decides the final destiny of the hydride ligand, which can be transferred to the central C atom of the allene to give an allyl product or to the terminal CH_2 fragment of the allene to give an alkenyl product.

Introduction

The reactions of the hydrazido-capped hydrido carbonyl triruthenium complex $[Ru_3(\mu\text{-}H)(\mu_3\text{-}\kappa^2\text{-}HNNMe_2)(CO)_9]$[1] (**1**; H_2NNMe_2 = 1,1-dimethylhydrazine) with a variety of terminal and internal alkynes without α-hydrogen atoms give trinuclear alkenyl derivatives that have their alkenyl ligands in edge-bridging or face-capping positions.[2] However, when the alkyne reagents have α-hydrogen atoms, the products contain face-capping alkenyl (**A** and **B** in Scheme 1) or edge-bridging allyl ligands (**C** and **D** in Scheme 1).[3] In all cases, the nature of the R groups of the alkyne reagents influences the regioselectivity of the reactions. Density functional theory (DFT) calculations have demonstrated that, for isomeric products, the allyl derivatives are thermodynamically more stable than their corresponding alkenyl isomers.[3]

In a recent work, studying the reactivity of compound **1** with conjugated dienes, we found that these unsaturated reagents afford allyl cluster derivatives in high yields (Scheme 2).[4] This synthetic approach represents an interesting alternative to the use of alkynes having α-hydrogen atoms as precursors to allyl ligands, especially if the alkyne required to make a particular allyl cluster complex is unknown or difficult to obtain, as happens for cyclic alkynes. A DFT study of the potential energy surface of the reaction pathway that gives the allyl cluster $[Ru_3(\mu_3\text{-}\kappa^2\text{-}HNNMe_2)(\mu\text{-}\kappa^3\text{-}C_6H_9)(\mu\text{-}CO)_2(CO)_6]$ (**E** in Scheme 2) from compound **1** and cyclohexa-1,3-diene allowed us to shed light on the mechanism by which cyclic 1,3-dienes are transformed into cyclic allyl ligands when they react with cluster **1**.[5]

We now report that, upon reaction with compound **1**, allenes also give trinuclear derivatives that contain edge-bridging allyl ligands and, in some instances, face-capping alkenyl ligands. We also report that, by means of DFT calculations, we have been able to model the mechanisms of the processes that render edge-bridging allyl or face-capping alkenyl derivatives from compound **1** and allenes. Some calculations aimed at explaining the preferred formation of *anti*-allyl versus the corresponding *syn*-allyl isomeric cluster products from **1** and substituted allenes are also reported.

Apart from those described in the above commented works,[3,4] triruthenium cluster complexes having organic

† Part of the Dietmar Seyferth Festschrift. Dedicated to Professor Dietmar Seyferth, to whom all organometallic chemists are indebted.

*To whom correspondence should be addressed. E-mail: jac@uniovi.es.

(1) Jenke, T.; Stoeckli-Evans, H.; Süss-Fink, G. *J. Organomet. Chem.* **1990**, *391*, 395.
(2) Cabeza, J. A.; del Río, I.; Fernández-Colinas, J. M.; García-Granda, S.; Martínez-Méndez, L.; Pérez-Carreño, E. *Chem.−Eur. J.* **2004**, *10*, 6265.
(3) Cabeza, J. A.; del Río, I.; García-Granda, S.; Martínez-Méndez, L.; Pérez-Carreño, E. *Chem.−Eur. J.* **2005**, *11*, 6040.
(4) Cabeza, J. A.; del Río, I.; Gille, M.; Goite, M. C.; Pérez-Carreño, E. *Organometallics* **2008**, *27*, 609.
(5) Cabeza, J. A.; Fernández-Colinas, J. M.; Pérez-Carreño, E. *Organometallics* **2009**, *28*, 4217.

 Published on Web 04/21/2010

Scheme 1

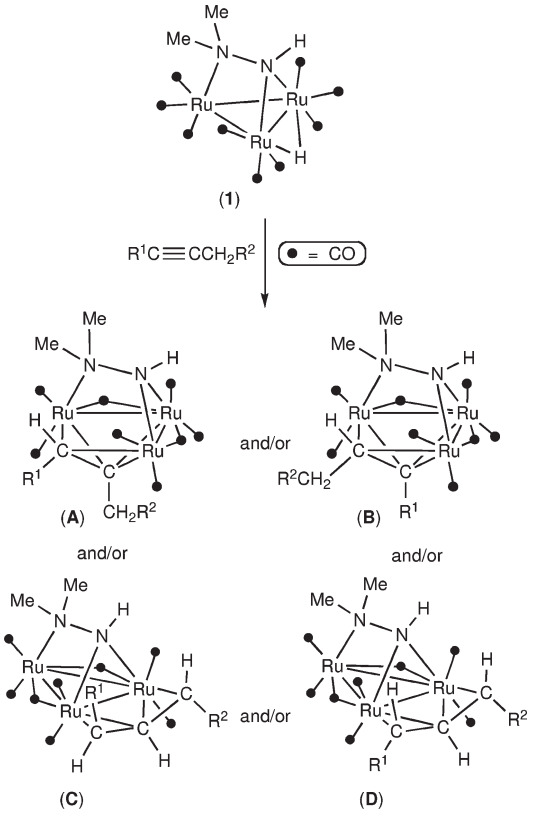

allyl ligands of the type $R^1R^2CCR^3CR^4R^5$ ($R^n \neq M$) are very rare, the only examples being $[Ru_3(\mu_3\text{-}\kappa^2\text{-}PPhCH_2PPh_2)(\mu\text{-}\kappa^3\text{-}C_3H_5)(CO)_8]$[6] and $[Ru_3(\mu_3\text{-}\kappa^5\text{-}HabqCHCHCHR)(\mu\text{-}CO)_2(CO)_6]$ (H_2abqH = 2-amino-7,8-benzoquinoline; R = H, C≡CSiMe$_3$),[7] which contain edge-bridging allyl ligands. Quite a few ruthenium cluster complexes containing 1,3-dimetalated allyl ligands ($MR^1CCR^2CR^3M$) are known.[8] One penta-[9] and one hexaruthenium[10] cluster have also been shown to contain edge-bridging organic allyl ligands.

In contrast, mononuclear ruthenium κ^3-allyl complexes have attracted much attention because they often participate in organometallic and catalytic reactions.[11] Detailed examples of insertion reactions of allenes into Ru−H bonds and the isomerism of some monoruthenium κ^3-allyl complexes have been published.[12] The chemistry involving insertion reactions of allenes into M−H and M−C bonds of mono- and binuclear complexes has been recently reviewed.[13]

Scheme 2

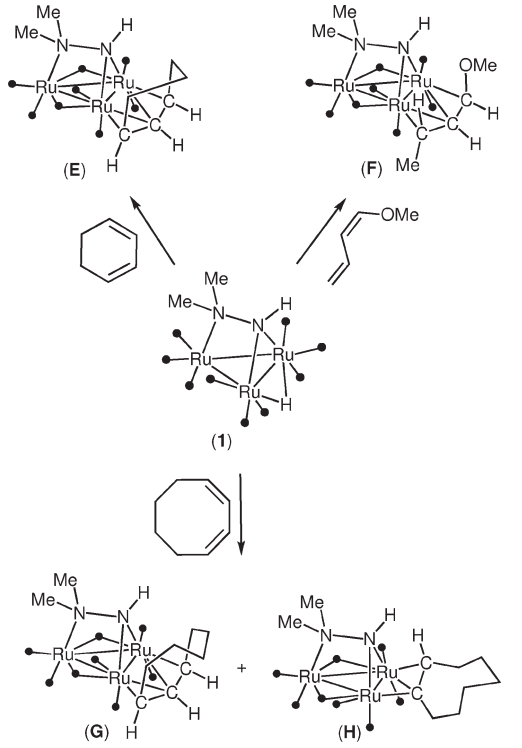

Scheme 3

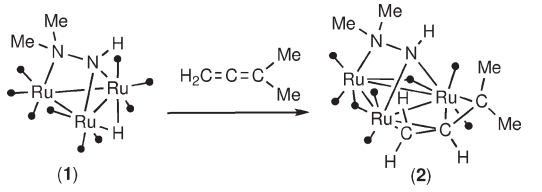

Results and Discussion

Reactions of Compound 1 with Allenes. With the aim of comparing the reactivity of various substituted allenes with compound **1**, two 1,1-disubstituted allenes (1,1-dimethylallene and 1-methyl-1-trimethylsilylallene) and two 1-monosubstituted allenes (ethyl 2,3-butadienoate and cyclohexylallene) were chosen as reagents. 1,3-Di-, tri-, and tetrasubstituted allenes and allene itself were not studied. The reactions were carried out in THF solution at reflux temperature (no reaction was observed at 20 °C), using a 1:1.2 compound **1** to allene molar ratio. Heating was stopped when IR and spot TLC inspection of the reacting solutions suggested the complete consumption of compound **1**. The reaction mixtures were separated by thin-layer chromatography (TLC) on silica gel. In all cases, some decomposition to untractable dark materials was observed on the TLC plates.

(6) Bruce, M. I.; Williams, M. L. *J. Organomet. Chem.* **1985**, *288*, C55.
(7) Cabeza, J. A.; del Río, I.; García-Granda, S.; Riera, V.; Suárez, M. *Organometallics* **2004**, *23*, 3501.
(8) (a) Evans, M.; Hursthouse, M.; Randall, E. W.; Rosenberg, E. *J. Chem. Soc., Chem. Commun.* **1972**, 545. (b) Castiglioni, M.; Milone, L.; Osella, D.; Vaglio, G. A.; Valle, M. *Inorg. Chem.* **1976**, *15*, 394. (c) Gervasio, G.; Osella, D.; Valle, M. *Inorg. Chem.* **1976**, *15*, 1176. (d) Beanan, L. R.; Rahman, Z. A.; Keister, J. B. *Organometallics* **1983**, *2*, 1062. (e) Beanan, L. R.; Keister, J. B. *Organometallics* **1985**, *4*, 1713. (f) Skinner, D. M.; Rosenberg, E.; Bracker-Novak, J.; Aime, S.; Osella, D.; Gobetto, R. *Organometallics* **1988**, *7*, 856. (g) Rao, K. M.; Angelici, R. J.; Young, V. G. *Inorg. Chim. Acta* **1992**, *198*, 211. (h) Doherty, S.; Corrigan, J. F.; Carty, A. J.; Sappa, E. *Adv. Organomet. Chem.* **1995**, *37*, 39. (i) Bruce, M. I.; Zaitseva, N. N.; Skelton, B. W.; White, A. H. *J. Chem. Soc., Dalton Trans.* **1999**, 2777. (j) Wong, W. Y.; Chan, S.; Wong, W. T. *J. Chem. Soc., Dalton Trans.* **1995**, 1497. (k) Gervasio, G.; Marabello, D.; King, P. J.; Sappa, E.; Secco, A. *J. Organomet. Chem.* **2003**, *671*, 385. (l) Cabeza, J. A.; da Silva, I.; del Río, I.; García-Granda, S.; Riera, V. *Inorg. Chim. Acta* **2003**, *347*, 107.
(9) Chihara, T.; Yamazaki, H. *J. Organomet. Chem.* **1992**, *428*, 169.
(10) Chihara, T.; Yamazaki, H. *J. Chem. Soc., Dalton Trans.* **1995**, 1369.
(11) See, for example: (a) Yamamoto, Y.; Nakagai, Y.; Itoh, K. *Chem.−Eur. J.* **2004**, *10*, 231. (b) Mbaye, M. D.; Demerseman, B.; Renaud, J. L.; Toupet, L.; Bruneau, C. *Angew. Chem., Int. Ed.* **2003**, *42*, 5066.
(12) (a) Xue, P.; Bi, S.; Sung, H. H. Y.; Williams, I. D.; Lin, Z.; Jia, G. *Organometallics* **2004**, *23*, 4735. (b) Bai, T.; Zhu, J.; Xue, P.; Sung, H. H.-Y.; Williams, I. D.; Ma, S.; Lin, Z.; Jia, G. *Organometallics* **2007**, *26*, 5581. (c) Xia, J.-L.; Wu, X.; Lu, Y.; Chen, G.; Jin, S.; Yu, G.; Liu, S.-H. *Organometallics* **2009**, *28*, 2701.
(13) Bai, T.; Ma, S.; Jia, G. *Coord. Chem. Rev.* **2009**, *253*, 423.

Scheme 4

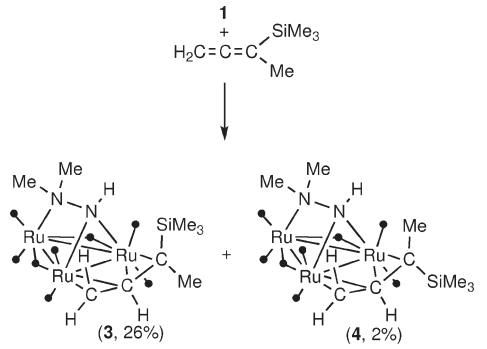

Scheme 5

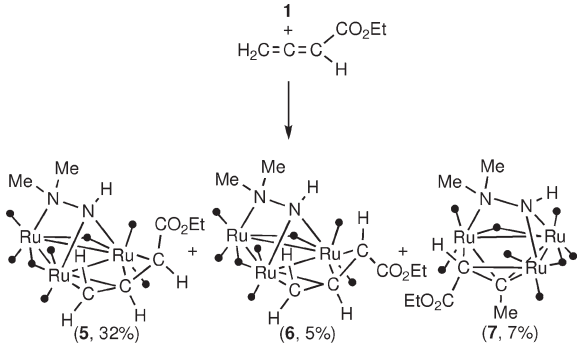

Scheme 6

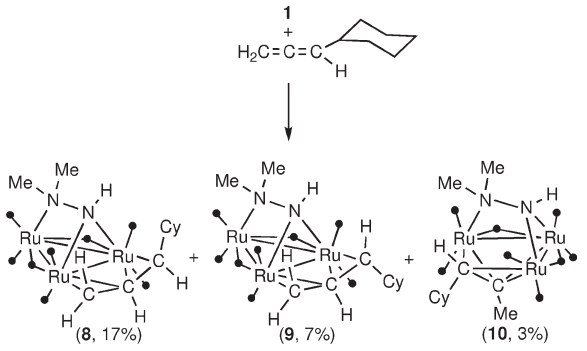

The reactivity results are shown in Schemes 3−6. All allenes used gave products having edge-bridging allyl ligands. The unsymmetrically substituted allenes gave mixtures of isomers having *anti*- (compounds **3**, **5**, **8**) or *syn*-allyl ligands (compounds **4**, **6**, **9**), the latter always being minor reaction products. While the 1,1-disubstituted allenes gave only allyl-bridged derivatives (compounds **2**−**4**; Schemes 3 and 4), the monosubstituted allenes also gave, in addition to the corresponding allyl derivatives (compounds **5**, **6**, **8**, **9**), a small amount of a face-capped alkenyl product (compounds **7**, **10**; Schemes 5 and 6).

Structural Characterization. The molecular structures of the allyl derivatives **2**, **3**, **6**, and **9** (Figures 1−4) have been determined by X-ray diffraction. For comparison purposes, as far as possible, a common atomic numbering scheme has been used. A selection of interatomic distances is given in Table 1. These structures are closely related. In the four cases, the hydrazido group caps the metal triangle in the same way as that found previously in complex **1**[1] and in most

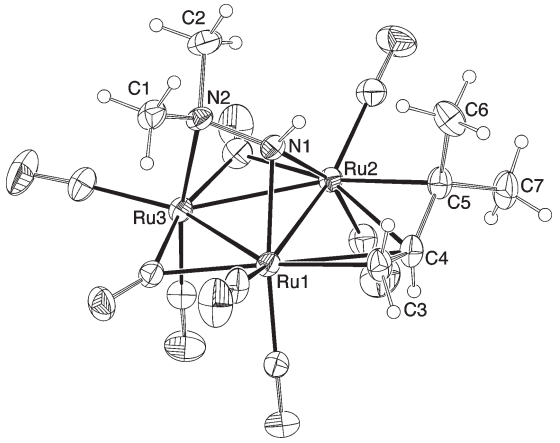

Figure 1. Molecular structure of compound **2**. Thermal ellipsoids are drawn at the 30% probability level.

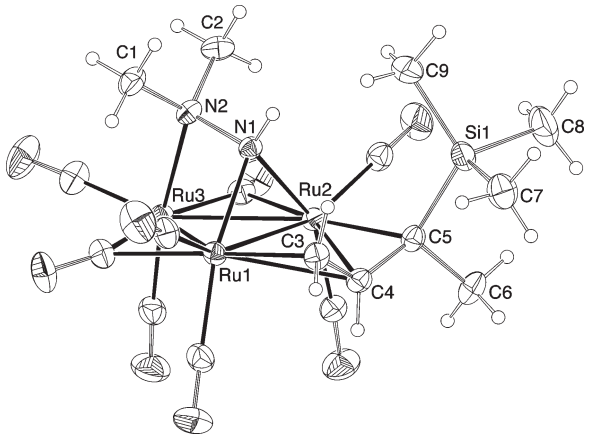

Figure 2. Molecular structure of compound **3**. Thermal ellipsoids are drawn at the 30% probability level.

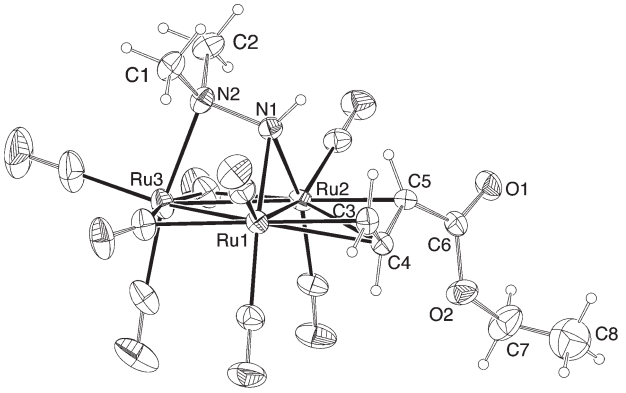

Figure 3. Molecular structure of compound **6**. Thermal ellipsoids are drawn at the 30% probability level.

of its derivatives.[2−4,14] The allyl ligand spans the same Ru−Ru edge as the amido fragment of the hydrazido group, being attached to Ru1 through the carbon atoms C3 and C4 and to Ru2 through C4 and C5, the distances from the

(14) (a) Cabeza, J. A.; del Río, I.; García-Granda, S.; Martínez-Méndez, L.; Riera, V. *J. Organomet. Chem.* **2002**, *663*, 227. (b) Cabeza, J. A.; del Río, I.; García-Granda, S.; Martínez-Méndez, L.; Riera, V. *Inorg. Chim. Acta* **2003**, *350*, 93. (c) Cabeza, J. A.; del Río, I.; García-Granda, S.; Martínez-Méndez, L.; Pérez-Carreño, E. *Organometallics* **2005**, *24*, 831.

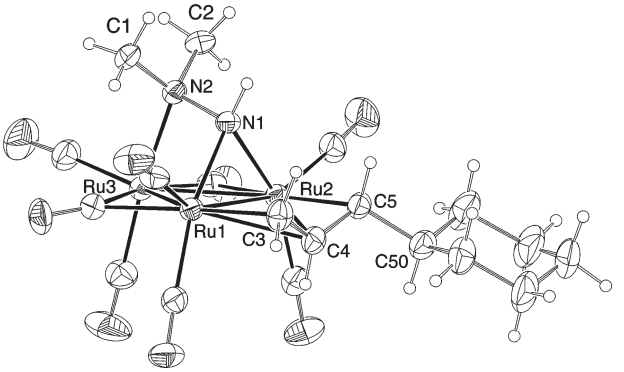

Figure 4. Molecular structure of compound **9**. Thermal ellipsoids are drawn at the 30% probability level.

Table 1. Selected Interatomic Distances (Å) in the μ-Allyl Derivatives 2, 3, 6, and 9

	2	3	6	9
Ru1−Ru2	2.7527(4)	2.7627(4)	2.7647(5)	2.7513(6)
Ru1−Ru3	2.7302(4)	2.7535(4)	2.7365(5)	2.7436(7)
Ru2−Ru3	2.7655(4)	2.7542(4)	2.7324(5)	2.7684(7)
N1−Ru1	2.129(3)	2.111(3)	2.136(4)	2.134(5)
N1−Ru2	2.134(3)	2.149(3)	2.118(4)	2.135(5)
N2−Ru3	2.208(3)	2.204(3)	2.215(4)	2.203(5)
C3−Ru1	2.181(4)	2.165(4)	2.193(4)	2.178(6)
C4−Ru1	2.642(4)	2.624(4)	2.538(4)	2.553(6)
C4−Ru2	2.487(4)	2.497(3)	2.589(4)	2.536(6)
C5−Ru2	2.242(4)	2.268(3)	2.184(4)	2.210(6)
C3−C4	1.426(6)	1.423(5)	1.383(7)	1.413(9)
C4−C5	1.422(6)	1.425(5)	1.427(6)	1.424(8)
C5−C6	1.532(6)	1.547(5)	1.463(6)	

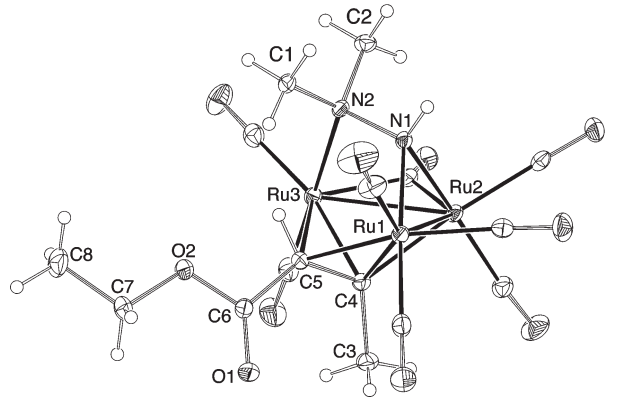

Figure 5. Molecular structure of compound **7**. Thermal ellipsoids are drawn at the 30% probability level.

central carbon atom C4 to Ru1 and Ru2 being 0.3−0.5 Å longer than those from C3 to Ru1 and C4 to Ru2. The dihedral angles between the planes defined by the allyl C3, C4, and C5 atoms and the Ru_3 triangle are 81.5(4)° in **2**, 79.9(4)° in **3**, 83.2(5)° in **6**, and 90.1(5)° in **9**. The *anti* arrangement and the large volume of the $SiMe_3$ group of compound **3** induce some asymmetry in the coordination of its allyl ligand, since the C5−Ru2 distance is 0.10 Å longer than the C3−Ru1 distance. The four compounds have eight CO ligands, two of which are bridging and six are terminal.

Table 2. Selected Interatomic Distances (Å) in the μ_3-Alkenyl Derivative 7

	distance		distance
Ru1−Ru2	2.7419(3)	Ru1−Ru3	3.7587(4)
Ru2−Ru3	2.7679(3)	N1−Ru1	2.105(2)
N1−Ru2	2.130(2)	N2−Ru3	2.233(2)
C4−Ru1	2.229(3)	C4−Ru2	2.246(3)
C4−Ru3	2.290(3)	C5−Ru1	2.238(3)
C5−Ru3	2.497(3)	C3−C4	1.530(4)
C4−C5	1.449(4)	C5−C6	1.480(4)

The Ru−Ru distances, ranging from 2.73 to 2.77 Å, confirm the presence of Ru−Ru single bonds.[15]

The X-ray structure of the alkenyl cluster **7** is depicted in Figure 5. A selection of interatomic distances is given in Table 2. In this case, the metal atoms are capped by the hydrazido ligand on one side and by the alkenyl ligand on the other side. The coordination of the alkenyl ligand is such that it is σ-bonded to Ru2 through C4 and π-bonded to both Ru1 and Ru3 through the carbon atoms of its double bond, C4 and C5. One bridging, one semibridging, and six terminal CO ligands complete the coordination shell. As the Ru1−Ru3 distance, 3.7587(4) Å, is outside the bonding range for Ru−Ru bonds,[15] this cluster represents an additional example of a rare group of 48-electron trinuclear clusters that contain only two metal−metal bonds, therefore not obeying the EAN rules, whose structures have been explained by molecular orbital calculations.[16] This compound is isostructural with the related alkenyl cluster $[Ru_3(\mu_3\text{-}\kappa^2\text{-}HNNMe_2)(\mu_3\text{-}\kappa^2\text{-}HCCHCO_2Me)(\mu\text{-}CO)_2(CO)_6]$, which was prepared by treating compound **1** with methyl propiolate.[2]

The NMR features of the allyl or alkenyl ligands of compounds **2**−**10** and the band patterns of the carbonyl stretching region of their IR spectra are comparable to those previously reported for other derivatives of compound **1** containing edge-bridging allyl[3,4] or face-capping alkenyl ligands[2] (as applicable).

DFT Calculations. Minimum-energy structure calculations (structure optimizations) were carried out by DFT methods at the B3LYP/LANL2DZ/6-31G(d,p) level. These calculations were performed on selected real molecules (products isolated in the present work) and on hypothetical ones with the aim of not only comparing their thermodynamic stability (important to rationalize the experimental results) but also assigning or confirming the structures of compounds for which no X-ray diffraction data were available. No simplified model compounds were used for these calculations. Roman numerals are assigned to all calculated structures, irrespectively of whether they correspond to isolated (also designated with Arabic numerals) or hypothetical compounds. The atomic coordinates of all these structures are given as Supporting Information. In the cases where both experimental (X-ray diffraction) and theoretical (DFT calculations) structural data were obtained, the structural parameters given by both methods are practically identical. This fact validates the calculations.

Figure 6 shows the relative energies of two families of compounds containing isomeric allyl and alkenyl products, formally derived from the 1,1-disubstituted allenes 1,1-dimethylallene and 1-methyl-1-trimethylsilylallene. In both cases, the allyl derivatives (structures **I**, **III**, and **IV**) are much more stable (by more than 26 kcal mol^{-1}) than their alkenyl

(15) The Ru−Ru distances in $[Ru_3(CO)_{12}]$ are in the range 2.8595 to 2.8515 Å: Churchill, M. R.; Hollander, F. J.; Hutchinson, J. P. *Inorg. Chem.* **1977**, *16*, 2655.

(16) Cabeza, J. A.; García-Alvarez, P.; Pérez-Carreño, E. *Organometallics* **2005**, *24*, 2000.

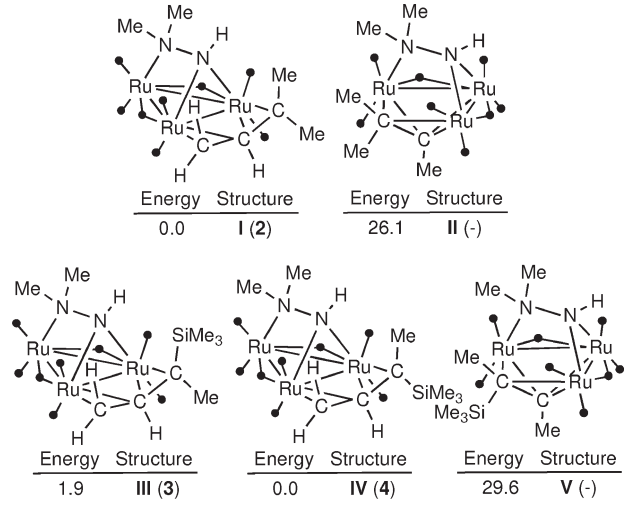

Figure 6. DFT-calculated relative energies (kcal mol^{-1}) of two groups of isomeric compounds derived from the 1,1-disubstituted allenes 1,1-dimethylallene (top) and 1-methyl-1-trimethylsilylallene (bottom). The energy of the most stable isomer of each group is 0.0 kcal mol^{-1}.

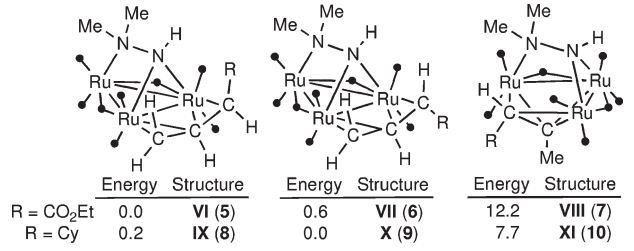

Figure 7. DFT-calculated relative energies (kcal mol^{-1}) of isomeric compounds derived from the monosubstituted allenes ethyl 2,3-butadienoate (R = CO_2Et) and cyclohexylallene (R = Cy). The energy of the most stable isomer of each group is 0.0 kcal mol^{-1}.

isomers (structures **II** and **V**). This explains why the reactions of compound **1** with 1,1-disubstituted allenes do not give products having face-capping alkenyl ligands.

The relative thermodynamic stability of families of isomeric compounds formally derived from the monosubstituted allenes ethyl 2,3-butadienoate and cyclohexylallene is given in Figure 7. It shows that the alkenyl derivatives (**VIII** and **XI**) are also less stable than their corresponding allyl isomers, but the differences are much smaller (7−12 kcal mol^{-1}) than those shown in Figure 6 for the products derived from 1,1-disubstituted allenes, probably because the steric hindrance between the alkenyl C−H and hydrazido N−Me fragments of **VIII** and **XI** is smaller than that of **II** and **V**. In fact, in **II** and **V**, such steric hindrance provokes a considerable structural distortion (lengthening of various Ru−C and Ru−Ru bonds) with respect to the "ideal" structures depicted in Figure 6, and this reduces the intrinsic thermodynamic stability of **II** and **V**.

Figures 6 and 7 also show that the allyl products having a bulky R group in an *anti* position (structures **III** and **IX**) are slightly less stable (< 2 kcal mol^{-1}) than their isomers having that group in a *syn* position (structures **IV** and **X**). In the case of structures **VI** and **VII**, the *anti* isomer **VI** is a bit more stable (0.2 kcal mol^{-1}) than the *syn* isomer **VII**, probably because in **VI** there is a hydrogen-bonding interaction (between the hydrazido NH group and carbonyl O atom of the ester group) that is missing in other *anti* products (structures **III** and **IX**).

As stated in the Introduction, it has been reported that allyl derivatives of compound **1** can also be prepared by treating **1** with alkynes having α-hydrogen atoms.[3] These reactions are thermodynamically controlled, giving their most stable derivatives, i.e., the *syn*-allyl isomers, as major reaction products.[3] However, as noted above, this is not the case for the reactions reported in this paper, which always give the *anti*-allyl derivatives as major products (product yields are given in Schemes 3−6), regardless of their relative thermodynamic stability with respect to the corresponding *syn*-allyl isomers.

To know whether the *anti*-allyl clusters **3** and **8** are intermediates in the formation of the more stable *syn*-allyl isomers **4** and **9**, respectively, the former compounds were heated in refluxing THF for 90 min, but no trace of the corresponding *syn* isomer was found in the resulting solutions. This finding suggests that the regioselectivity of the reactions of compound **1** with allenes is kinetically controlled and that the *anti*- and *syn*-allyl isomers are formed by independent reaction pathways.

To shed light on the reaction pathways that lead to allyl and alkenyl products from compound **1** and terminal allenes, mechanistic DFT studies were carried out at the B3LYP/LanL2DZ/6-31G(d,p) level of theory. To save computing time, the simplest allene, C_3H_4, was used as a model for these theoretical mechanistic studies.

The energy profile of the potential energy surface of the reaction that leads to the μ-allyl derivative $[Ru_3(\mu_3\text{-}\kappa^2\text{-}HNNMe_2)(\mu\text{-}\kappa^3\text{-}C_3H_5)(\mu\text{-}CO)_2(CO)_6]$ (**XII**) from the hydrido triruthenium cluster **1** and allene is displayed in Figure 8. The given energies are relative to those of the reactants (energy of **1** + energy of allene = 0.0 kcal mol^{-1}) and include the energy of none (**ts1**) or one CO molecule (**i1** to **XII**). The overall reaction, which is a five-step process, releases 21.5 kcal mol^{-1}. Its rate-determining step is the substitution of the allene for the corresponding CO ligand (**1** + allene → **i1** + CO). Table 3 shows the evolution of a selection of interatomic distances on going from **1** to **XII** through the corresponding intermediates (**i**) and transition states (**ts**).

As previously observed for other DFT-modeled CO substitution reactions on compound **1**,[5] the incorporation of the unsaturated reagent to the coordination shell of the trinuclear cluster occurs in an elemental step (**1** + C_3H_4 → **i1** + CO), in which the allene approaches the cluster Ru1 atom at the same time that the equatorial CO ligand C6−O6, which is *cis* to the bridging N-donor ligand (C6−Ru1 = 1.973 Å in **1**), is being released (C6−Ru1 = 3.507 Å in **ts1**). The long C3−Ru1 and C4−Ru1 distances of **ts1**, 3.939 and 4.174 Å, are shortened to 2.209 and 2.248 Å, respectively, in intermediate **i1**, which contains an η^2-allene in the same coordination site as that originally occupied by the released CO ligand. This is the step with the highest energy barrier of the whole reaction, 23.4 kcal mol^{-1}. The transfer of the hydride H1 atom to the allene C4 atom occurs in the second step, in which the η^2-allene ligand of **i1** is converted into a terminal η^3-allyl ligand in **i2** (C3−Ru1 = 2.393 Å, C4−Ru1 = 2.253 Å, C5−Ru1 = 2.276 Å). In transition state **ts2**, the hydride H1 atom approaches C4 (C4−H1 = 1.452 Å) while it detaches from Ru2 (H1−Ru1 = 1.763 Å, H1−Ru2 = 2.182 Å). The energy barrier of this step is moderate, 12.8 kcal mol^{-1} from **i1**. The following two steps (**i2** → **i3** → **i4**) should

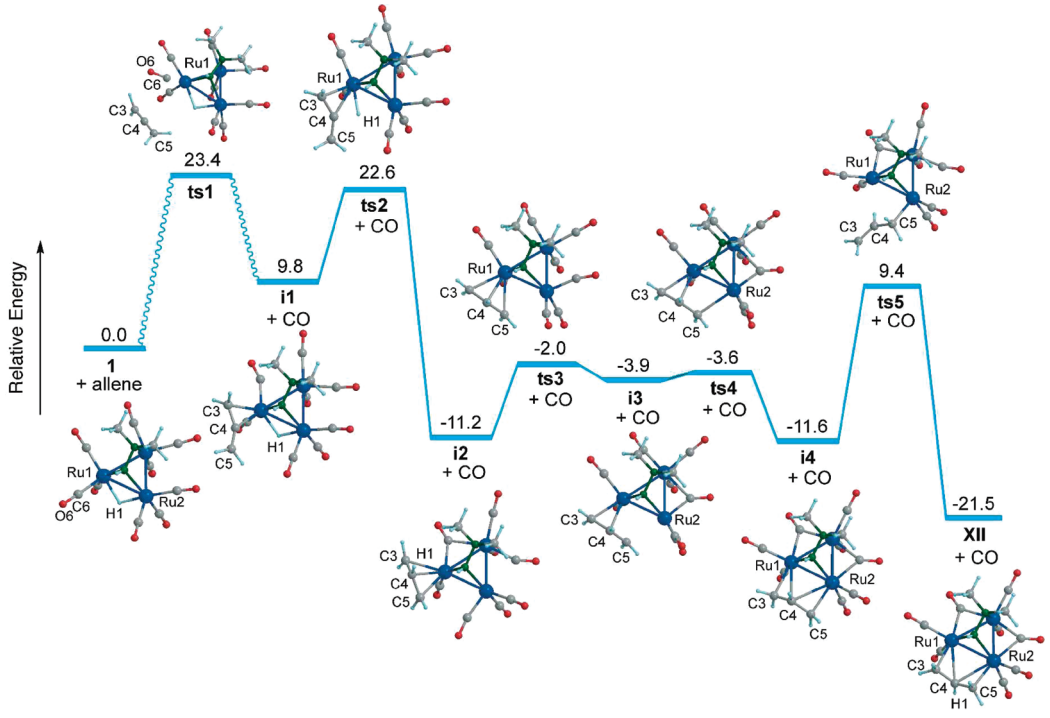

Figure 8. Relative energy profile (ΔE, kcal mol^{-1}) and DFT-optimized structures of the stationary points involved in the reaction **1** + allene → **XII** + CO.

Table 3. Computed Distances (Å) between Selected Atoms of the Stationary Points Involved in the Transformation of 1 into XII

atoms	**1** or allene	**ts1**	**i1**	**ts2**	**i2**	**ts3**	**i3**	**ts4**	**i4**	**ts5**	**XII**
C3−C4	1.307	1.309	1.404	1.411	1.397	1.397	1.405	1.402	1.408	1.336	1.422
C3−Ru1		3.939	2.193	2.209	2.393	2.358	2.313	2.322	2.305	3.995	2.223
C4−C5	1.307	1.307	1.325	1.330	1.424	1.424	1.415	1.424	1.408	1.492	1.422
C4−H1		3.893	2.874	1.452	1.088	1.089	1.090	1.090	1.090	1.110	1.087
C4−Ru1		4.174	2.117	2.248	2.253	2.284	2.306	2.313	2.751	3.000	2.647
C4−Ru2		5.350	3.953	3.578	4.447	3.553	3.357	3.304	2.751	2.936	2.647
C5−Ru1		4.778	3.238	3.423	2.276	2.464	2.590	2.652	3.520	3.450	3.482
C5−Ru2		5.285	4.385	4.168	3.869	2.915	2.718	2.615	2.305	2.146	2.223
C6−Ru1	1.973	3.507									
H1−Ru1	1.790	1.825	1.816	1.763	2.814	2.855	2.870	2.869	3.159	2.230	3.090
H1−Ru2	1.790	1.760	1.764	2.182	4.645	3.602	3.456	3.486	3.159	2.793	3.090

occur very readily because they have small energy barriers (9.2 and 0.3 kcal mol^{-1}, respectively). They involve a concomitant rearrangement of the equatorial CO ligands in the cluster and a slippage of the allyl ligand from a terminal position, attached to Ru1 in **i2**, to a bridging position, attached to Ru1 and Ru2 in **i4** (C3−Ru1 = C5−Ru2 = 2.305 Å, C4−Ru1 = C4−Ru2 = 2.751 Å). The last step (**i4** → **XII**) is energetically more demanding (the energy of **ts5** is 21.0 kcal mol^{-1} above that of **i4**) and involves (a) the conversion of the bridging allyl ligand of **i4** into a terminal -allyl ligand, (b) a rotation of the σ-allyl C3═C4 fragment about the C4−C5 single bond that separates the C4−H1 fragment from the bridging NH fragment, and (c) the recoordination of the C3═C4 fragment to Ru1 so that the allyl ligand symmetrically bridges the Ru1 and Ru2 atoms in XII (C3−Ru1 = C5−Ru2 = 2.223 Å, C4−Ru1 = C4−Ru2 = 2.647 Å).

The calculated energy profile of the process that leads to the face-capping alkenyl derivative [$Ru_3(\mu_3$-κ^2-HNNMe$_2$)-(μ_3-κ^2-MeCCH$_2$)(μ-CO)$_2$(CO)$_6$] (**XIII**) from compound **1** and allene is displayed in Figure 9, in which the given energies are relative to those of the reactants (energy of **1** + energy of allene = 0.0 kcal mol^{-1}) and include the energy of none (**ts6**) or one (**i5** to **XIII**) CO molecule. The overall reaction, which is a six-step process, releases 15.1 kcal mol^{-1}. Its rate-determining step is again the substitution of the allene for the corresponding CO ligand (**1** + allene → **i5** + CO). Table 4 shows the evolution of a selection of interatomic distances on going from **1** to **XIII** through the corresponding intermediates and transition states.

The first step is the incorporation of allene to the coordination shell of the trinuclear cluster (**1** + C_3H_4 → **i5** + CO). This step is very similar to that shown in Figure 8 for the reaction pathway that leads to the allyl product **XII**, involving the concomitant release of a CO ligand and the coordination of the allene, but differs in the approach of the allene ligand to Ru1. The long C4−Ru1 and C5−Ru1 distances in **ts6**, 4.124 and 3.979 Å, are shortened to 2.110 and 2.204 Å, respectively, in intermediate **i5**, in which C5 is the nearest allene carbon atom to the hydride ligand H1. This is the step with the highest energy barrier of the whole reaction, 23.5 kcal mol^{-1}. The second step involves the transfer of the hydride H1 atom to the allene C5 atom to give a terminal η^1-alkenyl ligand in **i6** (C4−Ru1 = 2.098 Å, C3−C4 = 1.339 Å, C4−C5 = 1.508 Å). In the transition state **ts7**, the hydride H1 atom approaches C5 (C5−H1 = 1.521 Å)

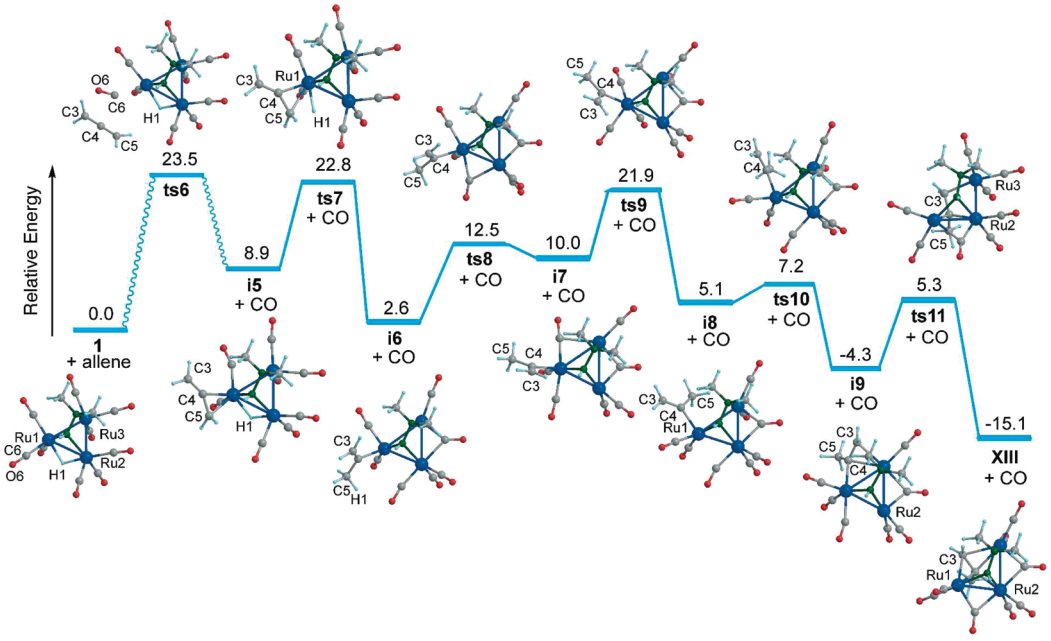

Figure 9. Relative energy profile (ΔE, kcal mol^{-1}) and DFT-optimized structures of the stationary points involved in the reaction **1** + allene → **XIII** + CO.

Table 4. Computed Distances (Å) between Selected Atoms of the Stationary Points Involved in the Transformation of 1 into XIII

atoms	**1** or allene	**ts6**	**i5**	**ts7**	**i6**	**ts8**	**i7**	**ts9**	**i8**	**ts10**	**i9**	**ts11**	**XIII**
C3−C4	1.307	1.307	1.324	1.326	1.339	1.336	1.337	1.340	1.340	1.347	1.394	1.435	1.397
C3−Ru1		4.656	3.213	3.227	3.026	3.066	3.087	3.100	3.130	3.061	3.194	2.937	2.483
C3−Ru3		7.354	5.739	5.748	5.433	5.489	5.453	5.185	4.849	3.738	2.325	2.241	2.470
C4−C5	1.307	1.309	1.402	1.422	1.508	1.507	1.508	1.510	1.503	1.518	1.524	1.519	1.527
C4−Ru1		4.124	2.110	2.101	2.098	2.167	2.174	2.212	2.104	2.089	2.148	2.166	2.350
C4−Ru2		5.718	4.546	4.273	4.166	4.337	4.603	4.507	4.561	4.380	4.053	2.285	2.277
C4−Ru3		6.799	4.672	4.807	4.941	4.979	4.794	4.351	3.636	3.168	2.317	2.759	2.390
C5−H1		3.509	2.959	1.521	1.094	1.096	1.097	1.096	1.095	1.097	1.097	1.098	1.094
C5−Ru1		3.979	2.204	2.301	3.077	3.169	3.174	3.261	2.975	3.085	3.173	3.236	3.444
C6−Ru1	1.973	3.516											
H1−Ru1	1.790	1.823	1.833	1.766	3.201	3.338	3.372	3.445	3.240	3.443	3.459	3.526	3.440
H1−Ru2	1.790	1.761	1.750	2.214	4.571	5.119	5.940	6.161	5.073	5.625	5.738	4.184	3.332
Ru1−Ru3	2.794	2.730	2.860	2.831	3.004	2.962	2.992	2.893	3.149	3.059	2.926	4.063	3.912

while it detaches from Ru2 (H1−Ru1 = 1.766 Å, H1−Ru2 = 2.212 Å). The energy barrier of this step is moderate, 12.9 kcal mol^{-1} from **i5**. The next two steps (**i6** → **i7** → **i8**) involve a rearrangement of the terminal alkenyl group and some CO ligands that places the alkenyl ligand closer to the Ru3 atom (C4−Ru3 = 3.636 Å in **i8**), while it is still terminally bonded to Ru1 (C4−Ru1 = 2.104 Å in **i8**), and creates a vacant coordination site in an equatorial position on the Ru3 atom of **i8**. This coordination vacancy is easily filled in the subsequent step (**i8** → **i9**), in which the alkenyl C3 and C4 carbon atoms bind the Ru3 atom, thus leading to an alkenyl-bridged species (in **i9**: C4−Ru1 = 2.148 Å, C4−Ru3 = 2.317 Å, C3−Ru3 = 2.325 Å). The last step (**i9** → **XIII**) involves a lengthening of the Ru1−Ru3 distance (from 2.926 Å in **i9** to 4.063 Å in **ts11** and 3.912 Å in **XIII**) and a concomitant movement of the alkenyl ligand from an edge-bridging (in **i9**) to a face-capping position (in **XIII**). The optimized structure of compound **XIII** (Figure 9, Table 4) resembles that determined by X-ray diffraction for compound **7** (Figure 5), since both have the alkenyl ligand σ-bonded to Ru2 through C4 and π-bonded to both Ru1 and Ru3 through the carbon atoms of its double bond, C4 and C5.

In Figures 8 and 9, we propose that the CO-substitution steps of both reactions **1** + allene → **i1** + CO or **i5** + CO follow bimolecular pathways. Going backward and forward along the reaction coordinate (IRC analysis) from the transition states **ts1** and **ts6**, it can be observed that the CO is released as the allene approaches the appropriate metal atom. However, as in **ts1** and **ts6** both the entering and leaving ligands are rather far away from the metal center considered (Tables 3 and 4), we also carried out calculations considering a typical dissociative pathway, in which the release of CO takes place prior to the coordination of the allene. They resulted in a slightly higher energy barrier (0.4−0.5 kcal mol^{-1}). In this context, a previous experimental kinetic study of the reaction of compound **1** with diphenylacetylene showed that that reaction is first order in the concentration of **1** and first order in alkyne concentration, having a $\Delta G^{\ddagger}$ of 28 kcal mol^{-1} in toluene at 318 K.[2] Additionally, kinetic measurements have also shown that the reactions of the anionic clusters $[Ru_3(\mu_3\text{-}\kappa^2\text{-Xpy})(\mu\text{-CO})_3(CO)_6]^-$ (X = S, NMe, NPh) with phosphine ligands to give CO-substitution products also follow a bimolecular mechanism.[17] All these data led us to propose that the CO-substitution (and rate-determining)

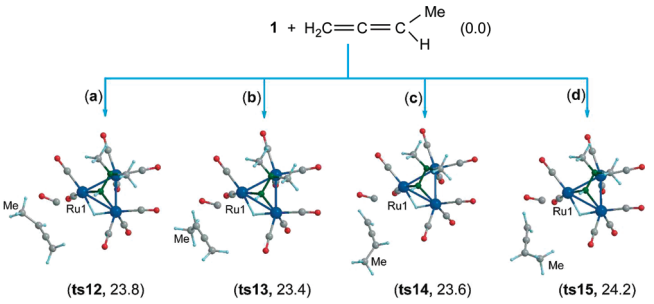

Figure 10. DFT-optimized structures and energies (ΔE, kcal mol^{-1}, relative to that of **1** + methylallene) of the four possible transition states found for the different approaches (a−d) of methylallene to compound **1** that can lead to allyl derivatives.

steps of the reactions of compound **1** with allenes follow bimolecular pathways.

The calculated energy barriers of both processes **1** + allene → **XII** + CO (Figure 8) or **XIII** + CO (Figure 9) are relatively high (23.4 and 23.5 kcal mol^{-1}), in agreement with the fact that these reactions do not take place at room temperature. As the remaining steps have lower activation barriers, these calculations also explain why no intermediates are observed when the reactions of **1** with allenes are monitored by IR spectroscopy.

The similar energy barriers of the CO-substitution steps (**ts1** and **ts6**) and the similar energy barriers of the steps associated with the *anti*-Markonikoff (**ts2**, Figure 8) and Markonikoff (**ts7**, Figure 9) migratory insertion of the coordinated allene into the corresponding Ru−H bond explain the low selectivity of the reactions of compound **1** with monosubstituted allenes, which give mixtures of allyl (arising from the *anti*-Markonikoff insertion) and alkenyl products (arising from the Markonikoff insertion).

As described above, the reactions of **1** with the asymmetrically substituted allenes 1-methyl-1-trimethylsilylallene and cyclohexylallene led to mixtures in which the major products are allyl derivatives that have their bulkiest substituent in an *anti* arrangement, despite being thermodynamically less stable than their *syn* counterparts (Figures 6 and 7). As this fact should have a kinetic origin, the reaction pathways that lead to the *syn*- and *anti*-allyl products should differ in their energy barriers, which, in turn, should be influenced by the nature of the R groups of the allene reagents. To check this line of reasoning, once we knew that the rate-determining step of these reactions is the incorporation of the allene to compound **1**, we decided to study this step by DFT methods using methylallene (buta-1,2-diene) as a model monosubstituted allene. Four different approaches of methylallene to compound **1**, which could lead to allyl products, were found (a−d in Figure 10), of which a and d would lead to the *syn* product and b and c would lead to the *anti* product if they follow a reaction pathway analogous to that shown for allene in Figure 8. However these four approaches resulted in very similar energy barriers (in the range 23.4−24.2 kcal mol^{-1}). We then reasoned that the methyl group might not be bulky enough to induce differences in the energy barriers of the four approaches (in fact, these barriers are very similar to that computed for unsubstituted allene, 23.4 kcal mol^{-1}, Figure 8). Consequently, we

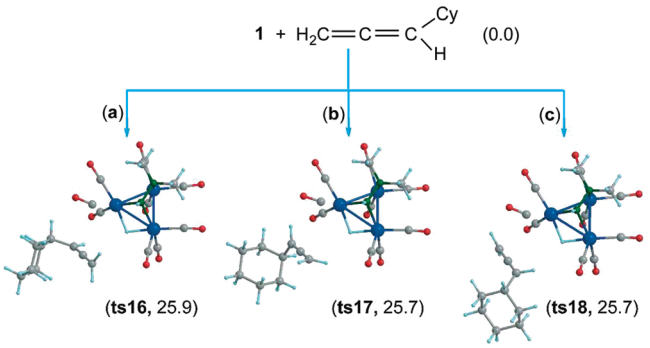

Figure 11. DFT-optimized structures and energies (ΔE, kcal mol^{-1}, relative to that of **1** + cyclohexylallene) of the three transition states found for the different approaches (a−c) of cyclohexylallene to compound **1** that can lead to allyl derivatives.

performed these calculations using cyclohexylallene as substituted allene, despite its cost in computing time, because this allene represents a real situation. In this case, approaches a−c were again found to have very similar energy barriers (in the range 25.7−25.9 kcal mol^{-1}, Figure 11), whereas no transition state corresponding to approach d was found, probably because in this approach the bulky cyclohexyl group impedes the allene from coming close to the metal atom. Therefore, the regioselectivity of the reactions of substituted allenes with compound **1** is not controlled by the rate-determining step of these processes but by other faster steps. Unfortunately, the fact that three different approaches of cyclohexylallene to compound **1** were possible and that each would lead to a different reaction pathway, coupled to computing limitations (working with molecules with three heavy atoms and such a large size requires very long computing times), led us to give up the investigation that would determine what individual step is responsible for the experimentally observed regioselectivity when *syn*- and *anti*-allyl isomeric products are possible. Nevertheless, it is now clear that such a step is not the rate-limiting step.

Conclusions

The reactivity of the hydrido carbonyl cluster complex **1** with allenes has been studied experimentally and computationally. While 1,1-disubstituted allenes give only allyl products, as mixtures of *syn* and *anti* isomers, monosubstituted allenes also give alkenyl derivatives as minor products.

This synthetic approach, which uses allenes as precursors to allyl ligands in carbonyl cluster complexes, represents an interesting alternative to the use of conjugated dienes and alkynes having α-hydrogen atoms as precursors to allyl ligands, especially when the 1,3-diene or the alkyne required to make a particular allyl ligand is unknown or difficult to prepare.

The reaction pathways that lead to allyl and alkenyl products from compound **1** have been established theoretically with the help of DFT methods, using allene (C_3H_4) as a model reagent. For both processes, the rate-determining step is the substitution of the allene for a CO ligand of **1**. The formation of an allyl or alkenyl product is determined by the way the allene coordinates to one of the cluster metal atoms, since this directs the result of a subsequent migratory insertion of the allene C=C bond into an Ru−H bond. The product is an allyl derivative if the original hydride ligand

(17) Shen, J. K.; Basolo, F.; Nombel, P.; Lugan, N.; Lavigne, G. *Inorg. Chem.* **1996**, *35*, 755.

ends in the allene central C atom (*anti*-Markonikoff insertion); otherwise, the product is an alkenyl derivative (Markonikoff insertion).

The alkenyl products are always thermodynamically less stable than the allyl products. In the case of the products derived from 1,1-disubstituted allenes, this difference is large enough to prevent the formation of alkenyl derivatives.

Some attempts have been made to theoretically address the experimentally observed preference for the formation of *anti*-allyl over *syn*-allyl products, even though, thermodynamically, the latter are a bit more stable than the former. Although this fact should have a kinetic origin, the rate-determining step of these processes is not responsible for the experimentally observed regioselectivity.

Experimental Section

General Data. Compound **1** was prepared by a published method.[1] The remaining reagents were purchased from commercial suppliers. Solvents were dried and distilled under nitrogen over sodium diphenyl ketyl (hydrocarbons, diethyl ether, THF) or CaH_2 (dichloromethane, 1,2-dichloroethane) just before use. The reactions were carried out under nitrogen, using Schlenk-vacuum line techniques, and were routinely monitored by solution IR spectroscopy (carbonyl stretching region) and spot TLC. IR spectra were recorded in solution on a Perkin-Elmer Paragon 1000 FT spectrophotometer. NMR spectra were run on a Bruker DPX-300 instrument, using the residual non-deuteriated solvent resonance ($CHCl_3$, δ_H = 7.26) and the solvent resonance ($CDCl_3$, δ_C = 77.16) as references for ^1H and ^{13}C, respectively. Microanalyses were obtained from the University of Oviedo Analytical Service. FAB mass spectra were obtained from the University of A Coruña Mass Spectrometric Service; data given refer to the most abundant molecular ion isotopomer.

[$Ru_3(\mu_3$-κ^2-HNNMe$_2$)(μ-κ^3-1,1-$Me_2C_3H_3$)(μ-CO)$_2$(CO)$_6$] (2). A solution of compound **1** (185 mg, 0.301 mmol) and 1,1-dimethylallene (34 μL, 0.336 mmol) in THF (30 mL) was stirred at reflux temperature for 30 min. The color changed from yellow to orange. The solvent was removed under reduced pressure, the residue was extracted into dichloromethane (1 mL), and the resulting solution was supported on silica gel TLC plates. Hexane/dichloromethane (1:1) eluted compound **2** as a yellow solid (81 mg, 41%). Anal. Calcd for $C_{15}H_{16}N_2O_8Ru_3$ (655.51): C, 27.48; H, 2.46; N, 4.27. Found: C, 27.44; H, 2.47; N, 4.19. (+)-FAB MS: m/z 657 $[M]^+$. IR (CH_2Cl_2): ν_{CO} 2052 (w), 2009 (vs), 1981 (s), 1960 (m), 1845 (w), 1805 (m). ^1H NMR ($CDCl_3$, 293 K): δ 3.29 (dd, J = 8.0, 4.0 Hz, 1 H; CHH), 2.55 (s, 3 H; CH_3), 2.11 (dd, J = 12.3, 8.0 Hz, 1 H; CH), 1.98 (s, 3 H; CH_3), 1.91 (s, 3 H; CH_3), 0.65 (s, 3 H; CH_3), 0.46 (s, 1 H; NH), 0.25 (dd, J = 12.3, 4.0 Hz, 1 H; CHH). $^{13}C\{^1H\}$ NMR ($CDCl_3$, 293 K): δ 254.3, 252.5, 200.1, 199.2, 198.8, 197.5, 196.5, 194.8 (8 COs), 59.5 (*C*), 59.3 (*C*H$_3$), 59.0 (*C*H), 55.9 (*C*H$_3$), 35.1 (*C*H$_3$), 23.7 (*C*H$_3$), 14.3 (*C*H$_2$).

[$Ru_3(\mu_3$-κ^2-HNNMe$_2$)(μ-κ^3-1-*anti*-SiMe$_3$-1-*syn*-Me-C_3H_3)(μ-CO)$_2$(CO)$_6$] (3) and [$Ru_3(\mu_3$-κ^2-HNNMe$_2$)(μ-κ^3-1-*syn*-SiMe$_3$-1-*anti*-Me-C_3H_3)(μ-CO)$_2$(CO)$_6$] (4). A solution of compound **1** (184 mg, 0.299 mmol) and 1-methyl-1-trimethylsilylallene (60 μL, 0.329 mmol) in THF (30 mL) was stirred at reflux temperature for 30 min. The color changed from yellow to orange. The solvent was removed under reduced pressure, the residue was extracted into dichloromethane (1 mL), and the resulting solution was supported on silica gel TLC plates. Repeated elution with hexane/dichloromethane (1.5:1) allowed the separation of two yellow bands. The first band afforded compound **3** (55 mg, 26%). The second band afforded compound **4** (5 mg, 2%). Data for **3**: Anal. Calcd for $C_{17}H_{22}N_2O_8Ru_3Si$ (713.67): C, 28.61; H, 3.11; N, 3.93. Found: C, 28.67; H, 3.15; N, 3.91. (+)-FAB MS: m/z 715 $[M]^+$. IR (CH_2Cl_2): ν_{CO} 2058 (s), 2011 (vs), 1987 (s), 1965 (m), 1847 (w), 1803 (m). ^1H NMR ($CDCl_3$, 293 K): δ 3.62 (dd, J = 7.6, 4.3 Hz, 1 H; CHH), 2.25 (s, 3 H; CH_3), 2.19 (dd, J = 13.1, 7.6 Hz, 1 H; CH), 1.96 (s, 3 H; CH_3), 1.94 (s, 3 H; CH_3), 0.90 (s, 1 H; NH), 0.02 (s, 9 H; CH_3), −0.35 (dd, J = 13.1, 4.3 Hz, 1 H; CHH). $^{13}C\{^1H\}$ NMR ($CDCl_3$, 293 K): δ 254.0, 250.9, 199.3, 199.1, 199.0, 196.7, 196.1, 194.4 (8 COs), 63.3 (*C*H), 59.2 (*C*H$_3$), 58.4 (*C*H$_3$), 52.8 (*C*), 33.7 (*C*H$_3$), 18.0 (*C*H$_2$), 1.6 (*C*H$_3$). Data for **4**: Anal. Calcd for $C_{17}H_{22}N_2O_8Ru_3Si$ (713.67): C, 28.61; H, 3.11; N, 3.93. Found: C, 28.69; H, 3.17; N, 3.90. (+)-FAB MS: m/z 715 $[M]^+$. IR (CH_2Cl_2): ν_{CO} 2056 (s), 2011 (vs), 1987 (s), 1966 (m), 1845 (w), 1802 (m). ^1H NMR ($CDCl_3$, 293 K): δ 3.53 (dd, J = 7.6, 3.5 Hz, 1 H; CHH), 2.18 (dd, J = 12.5, 7.6 Hz, 1 H; CH), 2.03 (s, 3 H; CH_3), 1.90 (s, 3 H; CH_3), 0.60 (dd, J = 12.5, 3.5 Hz, 1 H; CHH), 0.59 (s, 1 H; NH), 0.44 (s, 9 H; CH_3), 0.35 (s, 3 H; CH_3). $^{13}C\{^1H\}$ NMR ($CDCl_3$, 293 K): δ 253.1, 252.4, 199.8, 198.9, 198.5, 197.3, 196.2, 194.2 (8 COs), 42.1(*C*), 59.1 (*C*H$_3$), 58.8 (*C*H), 57.5 (*C*H$_3$), 42.1 (*C*), 18.9 (*C*H$_2$), 18.5 (*C*H$_3$), 0.29 (*C*H$_3$).

[$Ru_3(\mu_3$-κ^2-HNNMe$_2$)(μ-κ^3-1-*anti*-$C_3H_4CO_2$Et)(μ-CO)$_2$(CO)$_6$] (5), [$Ru_3(\mu_3$-κ^2-HNNMe$_2$)(μ-κ^3-1-*syn*-$C_3H_4CO_2$Et)(μ-CO)$_2$(CO)$_6$] (6), and [$Ru_3(\mu_3$-κ^2-HNNMe$_2$)(μ_3-κ^2-MeCCHCO$_2$Et)(μ-CO)$_2$(CO)$_6$] (7). A solution of compound **1** (228 mg, 0.370 mmol) and ethyl 2,3-butadienoate (50 μL, 0.409 mmol) in THF (30 mL) was stirred at reflux temperature for 30 min. The color changed from yellow to orange. The solvent was removed under reduced pressure, the residue was extracted into dichloromethane (1 mL), and the resulting solution was supported on silica gel TLC plates. Repeated elution with hexane/dichloromethane (2:1) allowed the separation of three yellow bands, which were extracted to give, in order of elution, compounds **5** (87 mg, 32%), **7** (18 mg, 7%), and **6** (12 mg, 5%). Data for **5**: Anal. Calcd for $C_{16}H_{16}N_2O_{10}Ru_3$ (699.52): C, 27.47; H, 2.31; N, 4.00. Found: C, 27.50; H, 2.38; N, 3.96. (+)-FAB MS: m/z 701 $[M]^+$. IR (CH_2Cl_2): ν_{CO} 2062 (s), 2023 (vs), 1993 (s), 1973 (m), 1856 (w), 1808 (m). ^1H NMR ($CDCl_3$, 293 K): δ 4.46 (d, J = 8.4 Hz, 1 H; CHH), 3.95 (q, J = 7.1 Hz, 2 H; CH_2), 3.46 (d, J = 8.4 Hz, 1 H; CHH), 2.46 (dt, J = 12.8, 8.0 Hz, 1 H; CH), 2.02 (s, 3 H; CH_3), 1.84 (s, 3 H; CH_3), 1.38 (s, 1 H; NH), 1.29 (m, 4 H). $^{13}C\{^1H\}$ NMR ($CDCl_3$, 293 K): δ 251.3, 247.6, 198.2, 197.7, 196.7, 195.9, 195.2, 194.0 (CO_s), 174.9 (*C*O$_2$Et), 60.3 (*C*H$_2$), 58.6 (*C*H$_3$), 58.4 (*C*H), 55.3 (*C*H$_3$), 24.5 (*C*H), 23.3 (*C*H$_2$), 14.1 (*C*H$_3$). Data for **6**: Anal. Calcd for $C_{16}H_{16}N_2O_{10}Ru_3$ (699.52): C, 27.47; H, 2.31; N, 4.00. Found: C, 27.52; H, 2.37; N, 3.97. (+)-FAB MS: m/z 699 $[M - 2]^+$. IR (CH_2Cl_2): ν_{CO} 2065 (s), 2026 (vs), 1996 (s), 1976 (m), 1857 (w), 1811 (m). ^1H NMR ($CDCl_3$, 293 K): δ 4.48, 4.35 (m, 2 H; CH_2), 3.63 (dd, J = 7.9, 2.3 Hz, 1 H; CHH), 2.90 (m, 1 H; CH), 1.94 (s, 3 H; CH_3), 1.93 (s, 3 H; CH_3), 1.42 (t, J = 7.1 Hz, 1 H; CH_3), 0.92 (d, J = 10.9 Hz, 1 H; CH), 0.46 (s, 1 H; NH), 0.14 (dd, J = 12.4, 2.3 Hz, 1 H; CHH). $^{13}C\{^1H\}$ NMR ($CDCl_3$, 293 K): δ 251.1, 247.8, 197.8, 197.6, 196.3, 195.9, 195.6, 193.7 (8 COs), 177.7 (*C*O$_2$Et), 61.1 (*C*H$_2$), 58.9 (*C*H$_3$), 58.7 (*C*H), 53.4 (*C*H$_3$), 38.7 (*C*H), 25.6 (*C*H$_2$), 14.4 (*C*H$_3$). Data for **7**: Anal. Calcd for $C_{16}H_{16}N_2O_{10}Ru_3$ (699.52): C, 27.47; H, 2.31; N, 4.00. Found: C, 27.50; H, 2.35; N, 3.97. (+)-FAB MS: m/z 699 $[M - 2]^+$. IR (CH_2Cl_2): ν_{CO} 2075 (w), 2032 (s), 2011 (s), 1962 (m), 1799 (w, br). ^1H NMR ($CDCl_3$, 293 K): δ 4.30 (m, 2 H; CH_2), 2.71 (s, 3 H; CH_3), 2.64 (s, 3 H; CH_3), 2.31 (s, 1 H; CH), 2.20 (s, 3 H; CH_3), 2.12 (s, 1 H; NH), 1.37 (t, J = 7.2 Hz, 3 H; CH_3). $^{13}C\{^1H\}$ NMR ($CDCl_3$, 293 K): δ 232.4, 217.4, 199.3, 197.9, 196.9, 196.7, 196.7, 193.7 (8 COs), 168.9 (*C*O$_2$Et), 138.2 (*C*), 61.6 (*C*H), 61.5 (*C*H$_2$), 57.6 (*C*H$_3$), 51.3 (*C*H$_3$), 38.1 (*C*H$_3$), 14.4 (*C*H$_3$).

[$Ru_3(\mu_3$-κ^2-HNNMe$_2$)(μ-κ^3-1-*anti*-C_3H_4Cy)(μ-CO)$_2$(CO)$_6$] (8), [$Ru_3(\mu_3$-κ^2-HNNMe$_2$)(μ-κ^3-1-*syn*-C_3H_4Cy)(μ-CO)$_2$(CO)$_6$] (9), and [$Ru_3(\mu_3$-κ^2-HNNMe$_2$)(μ_3-κ^2-MeCCHCy)(μ-CO)$_2$(CO)$_6$] (10). A solution of compound **1** (145 mg, 0.236 mmol) and cyclohexylallene (40 μL, 0.259 mmol) in THF (30 mL) was stirred at reflux temperature for 30 min. The color changed from yellow to orange. The solvent was removed under reduced pressure, the

Table 5. Crystal, Measurement, and Refinement Data for the Compounds Studied by X-ray Diffraction

	2	**3**	**6**·$(C_2H_4Cl_2)_{0.5}$	**7**·$(CH_2Cl_2)_{0.5}$	**9**
formula	$C_{15}H_{16}N_2O_8Ru_3$	$C_{17}H_{22}N_2O_8Ru_3Si$	$C_{16}H_{16}N_2O_{10}Ru_3 \cdot (C_2H_4Cl_2)_{0.5}$	$C_{16}H_{16}N_2O_{10}Ru_3 \cdot (CH_2Cl_2)_{0.5}$	$C_{19}H_{22}N_2O_8Ru_3$
fw	655.52	713.67	748.99	740.97	709.60
cryst syst	orthorhombic	monoclinic	monoclinic	monoclinic	orthorhombic
space group	$P2_12_1$	$P2_1/c$	$C2/c$	$C2/c$	$Pbca$
a, Å	9.4617(1)	9.5519(2)	33.4604(7)	21.0688(5)	11.2152(2)
b, Å	13.8364(2)	9.4221(2)	12.8129(2)	15.2472(4)	12.4955(2)
c, Å	15.8330(2)	26.6438(6)	27.9386(6)	17.7538(4)	34.8874(6)
α, deg	90	90	90	90	90
β, deg	90	95.450(1)	122.358(1)	123.904(1)	90
γ, deg	90	90	90	90	90
V, Å^3	2072.79(5)	2387.07(9)	10118.0(3)	4733.5(2)	4889.10(14)
Z	4	4	8	4	8
F(000)	1264	1392	5808	2864	2768
D_{calcd}, g cm^{-3}	2.104	1.986	1.967	2.079	1.925
μ(Mo Kα), mm^{-1}	2.200	1.967	1.924	2.055	1.874
cryst size, mm	0.25 × 0.20 × 0.10	0.27 × 0.22 × 0.10	0.32 × 0.30 × 0.25	0.30 × 0.12 × 0.12	0.17 × 0.07 × 0.05
temp, K	293(2)	293(2)	293(2)	150(2)	293(2)
θ limits, deg	1.95 to 25.35	1.54 to 25.34	1.44 to 25.35	1.77 to 25.35	1.17 to 25.36
min./max. h	0/11	0/11	0/40	0/25	0/13
min./max. k	0/16	0/11	0/15	0/18	0/15
min./max. l	−18/19	−32/31	−33/28	−21/17	0/42
no. of collected rflns	20 210	16 596	23 055	13 532	48 532
no. of unique rflns	3792	4358	9260	4328	4474
no. of reflns with $I > 2\sigma(I)$	3715	3969	7740	4035	3532
no. of params/restraints	254/1	292/2	590/0	313/0	292/1
GOF on F^2	1.060	1.035	1.018	1.014	1.071
R_1 (on F, $I > 2\sigma(I)$)	0.0235	0.0248	0.0359	0.0191	0.0331
wR_2 (on F^2, all data)	0.0645	0.0907	0.1107	0.0714	0.1348
max./min. Δρ, e Å^{-3}	0.950/-2.079	0.874/-1.930	1.556/-1.657	0.957/-0.918	1.313/-1.671

residue was extracted into dichloromethane (1 mL), and the resulting solution was supported on silica gel TLC plates. Elution with hexane/dichloromethane (1:1) separated three yellow bands, which were extracted to give, in order of elution, compounds **8** (29 mg, 17%), **9** (11 mg, 7%), and **10** (3 mg, 2%). Data for **8**: Anal. Calcd for $C_{19}H_{22}N_2O_8Ru_3$ (709.60): C, 32.16; H, 3.12; N, 3.95. Found: C, 32.19; H, 3.16; N, 3.92. (+)-FAB MS: m/z 711 [M]$^+$. IR (CH_2Cl_2): ν_{CO} 2058 (s), 2011 (vs), 1986 (s), 1964 (m), 1847 (w), 1803 (w). ^{1}H NMR ($CDCl_3$, 293 K): δ 4.57 (t, J = 9.4 Hz, 1 H; CH), 3.25 (m, 1 H; CHH), 1.91 (s, 6 H; CH_3), 2.23−0.75 (m, 12 H), 0.63 (dd, J = 12.4, 3.8 Hz, 1 H; CHH), 0.46 (s, 1 H; NH). ^{13}C{^{1}H} NMR ($CDCl_3$, 293 K): δ 253.0, 252.3, 198.9, 198.8, 197.5, 196.9, 196.4, 194.6 (8 COs), 59.3 (CH_3), 58.8 (CH), 55.5 (CH_3), 50.8 (CH), 38.3 (CH_2), 36.4 (CH), 35.2 (CH_2), 26.8 (CH_2), 26.6 (CH_2), 26.1 (CH_2), 13.9 (CH_2). Data for **9**: Anal. Calcd for $C_{19}H_{22}N_2O_8Ru_3$ (709.60): C, 32.16; H, 3.12; N, 3.95. Found: C, 32.20; H, 3.16; N, 3.94. (+)-FAB MS: m/z 683 [M − CO]$^+$. IR (CH_2Cl_2): ν_{CO} 2058 (s), 2013 (vs), 1985 (s), 1963 (m), 1847 (w), 1803 (w). ^{1}H NMR ($CDCl_3$, 293 K): δ 3.61 (dd, J = 7.7, 3.1 Hz, 1 H; CHH), 1.93 (s, 3 H; CH_3), 1.89 (s, 3 H; CH_3), 2.76−0.77 (m, 13 H), 0.29 (s, 1 H; NH), −0.39 (dd, J = 11.9, 3.1 Hz, 1 H; CHH). ^{13}C{^{1}H} NMR ($CDCl_3$, 293 K): δ 59.9 (CH), 59.2 (CH_3), 58.8 (CH_3), 53.9 (CH_2), 46.5 (CH), 36.1 (CH_2), 27.4 (CH_2), 27.3 (CH_2), 26.8 (CH_2), 14.6 (CH) (CO signals not observed due to insufficient concentration of the sample). Data for **10**: Anal. Calcd for $C_{19}H_{22}N_2O_8Ru_3$ (709.60): C, 32.16; H, 3.12; N, 3.95. Found: C, 32.18; H, 3.15; N, 3.91. (+)-FAB MS: m/z 711 [M]$^+$. IR (CH_2Cl_2): ν_{CO} 2056 (w), 2014 (s), 1984 (m), 1953 (m), 1847 (w), 1815 (w). ^{1}H NMR ($CDCl_3$, 293 K): δ 3.06 (d, J = 5.4 Hz, 1 H; CH), 2.61 (s, 3 H; CH_3), 2.17 (s, 3 H; CH_3), 2.11 (s, 1 H; CH_3), 2.36, 1.86, 1.40 (m, 11 H), 1.75 (s, 1 H; NH). ^{13}C{^{1}H} NMR ($CDCl_3$, 293 K): δ 239.5, 230.7, 201.8, 200.5, 199.2, 198.8, 197.2, 195.8 (8 COs), 127.6 (C), 86.1 (CH), 60.7 (CH_3), 56.8 (CH_3), 39.9 (CH_2), 38.6 (CH_2), 35.4 (CH), 27.0 (CH_2), 26.7 (CH_2), 25.6 (CH_2).

X-ray Diffraction Analyses. Selected crystal and refinement data are given in Table 5. Diffraction data for **2**, **3**, **6**·$(C_2H_4Cl_2)_{0.5}$, **7**·$(CH_2Cl_2)_{0.5}$, and **9** were collected on a Nonius Kappa-CCD diffractometer, using graphite-monochromated Mo Kα radiation. A semiempirical absorption correction was performed with SORTAV.[18] Structures were solved by Patterson interpretation using the program DIRDIF-96.[19] Isotropic and full matrix anisotropic least-squares refinements were carried out with SHELXL-97.[20] Except the carbon atom C(8) of compound **6**, all non-H atoms were refined anisotropically. Two crystallography independent cluster molecules were found in the asymmetric unit of **6**·$(C_2H_4Cl_2)_{0.5}$. Only the carbon and chlorine atoms of a disordered dichloromethane molecule were refined and included in the final model of **7**·$(CH_2Cl_2)_{0.5}$. The molecular plots were made with the PLATON program package.[21] The WINGX program system[22] was used throughout the structure determinations. CCDC deposition numbers: 766565−766569.

Computational Details. Density functional theory calculations were carried out using the Becke's three-parameter hybrid exchange−correlation functional[23] and the B3LYP nonlocal gradient correction.[24] The LanL2DZ basis set, with relativistic effective core potentials, was used for the Ru atoms.[25] The basis set 6-31G, with addition of (d,p)-polarization,[26] was used for the remaining atoms. It has been previously shown that the B3LYP/LanL2DZ/6-31G(d,p) approximation used in this paper provides an acceptable balance between accuracy and computing time when working with large molecules containing heavy atoms.[27] Crystallographically determined structures provided

(18) Blessing, R. H. *Acta Crystallogr.* **1995**, *A51*, 33.
(19) Beurskens, P. T.; Beurskens, G.; de Gelder, R.; Smits, J. M. M.; García-Granda, S.; Gould, R. O. *The DIRDIF Program System, version 2008.3*; Crystallography Laboratory, University of Nijmegen: Nijmegen, The Netherlands, 2008.
(20) *SHELXL*, version 2008: Sheldrick, G. M. *Acta Crystallogr.* **2008**, *A64*, 112.
(21) Spek, A. L. *PLATON: A Multipurpose Crystallographic Tool, version 1.15*; University of Utrecht: Utrecht, The Netherlands, 2008.
(22) *WinGX*, version 1.80.05 (2009): Farrugia, L. J. *J. Appl. Crystallogr.* **1999**, *32*, 837.
(23) Becke, A. D. *J. Chem. Phys.* **1993**, *98*, 5648.
(24) Lee, C.; Yang, W.; Parr, R. G. *Phys. Rev. B* **1988**, *37*, 785.
(25) Hay, P. J.; Wadt, W. R. *J. Chem. Phys.* **1985**, *82*, 299.
(26) Hariharan, P. C.; Pople, J. A. *Theor. Chim. Acta* **1973**, *28*, 213.

initial geometries for the optimization of compounds **1**[1] and the trinuclear allyl and alkenyl derivatives. For the mechanistic studies, IRC calculations were used to verify that the transition states found were connected to the proposed intermediates, reactants, or products. Calculation of analytical frequencies for all stationary points provided one imaginary eigenvalue for transition states and positive eigenvalues for reactants, products, and intermediates. All energies given in this article are potential energies calculated in gas phase. All calculations were carried out without symmetry constraints utilizing the Gaussian03 package.[28]

Acknowledgment. This work has been supported by the European Union (FEDER grants) and the Spanish MICINN (projects CTQ2007-60865 and MAT2006-1997). We also thank Xunta de Galicia for a fellowship to D.V.-G.

Supporting Information Available: Atomic coordinates of all DFT-optimized structures and crystallographic data in CIF format for the compounds studied by X-ray diffraction. This material is available free of charge via the Internet at http://pubs.acs.org.

(27) (a) Musaev, D. G.; Nowroozi-Isfahani, T.; Morokuma, K.; Rosenberg, E.; Abedin, J.; Hardcastle, K. I. *Organometallics* **2005**, *24*, 5973. (b) Musaev, D. G.; Nowroozi-Isfahani, T.; Morokuma, K.; Rosenberg, E. *Organometallics* **2006**, *25*, 203. (c) Nowroozi-Isfahani, T.; Musaev, D. G.; Morokuma, K.; Rosenberg, E. *Inorg. Chem.* **2006**, *45*, 4963. (d) Cabeza, J. A.; Pérez-Carreño, E. *Organometallics* **2008**, *27*, 4697. (e) Cabeza, J. A.; del Río, I.; Goite, M. C.; Pérez-Carreño, E.; Pruneda, V. *Chem.—Eur. J.* **2009**, 7339. (f) Cabeza, J. A.; del Río, I.; Pérez-Carreño, E.; Sánchez-Vega, M. G.; Vázquez-García, D. *Angew. Chem., Int. Ed.* **2009**, *48*, 555.

(28) Frisch, M. J.; Trucks, G. W.; Schlegel, H. B.; Scuseria, G. E.; Robb, M. A.; Cheeseman, J. R.; Montgomery, J. A., Jr.; Vreven, T.; Kudin, K. N.; Burant, J. C.; Millam, J. M.; Iyengar, S. S.; Tomasi, J.; Barone, V.; Mennucci, B.; Cossi, M.; Scalmani, G.; Rega, N.; Petersson, G. A.; Nakatsuji, H.; Hada, M.; Ehara, M.; Toyota, K.; Fukuda, R.; Hasegawa, J.; Ishida, M.; Nakajima, T.; Honda, Y.; Kitao, O.; Nakai, H.; Klene, M.; Li, X.; Knox, J. E.; Hratchian, H. P.; Cross, J. B.; Adamo, C.; Jaramillo, J.; Gomperts, R.; Stratmann, E. R.; Yazyev, O.; Austin, A. J.; Cammi, R.; Pomelli, C.; Ochterski, J. W.; Ayala, P. Y.; Morokuma, K.; Voth, G. A.; Salvador, P.; Dannenberg, J. J.; Zakrzewski, V. G.; Dapprich, S.; Daniels, A. D.; Strain, M. C.; Farkas, O.; Malick, D. K.; Rabuck, A. D.; Raghavachari, K.; Foresman, J. B.; Ortiz, J. V.; Cui, Q.; Baboul, A. G.; Clifford, S.; Cioslowski, J.; Stefanov, B. B.; Liu, G.; Liashenko, A.; Piskorz, P.; Komaromi, I.; Martin, R. L.; Fox, D. J.; Keith, T.; Al-Laham, M. A.; Peng, C. Y.; Nanayakkara, A.; Challacombe, M.; Gill, P. M. W.; Johnson, B.; Chen, W.; Wong, M.; Gonzalez, W. C.; Pople, J. A. *Gaussian-03, Revision C2*; Gaussian Inc.: Wallingford, CT, 2004.